Activity versus selectivity in photocatalysis : morphological or electronic properties tipping the scale

Activity *versus* selectivity in photocatalysis:

Morphological or electronic properties tipping the scale

Maarten Keulemans[1,2], *Sammy W. Verbruggen*[1,2*], *Birger Hauchecorne*[1], *Johan A. Martens*[2] *and Silvia Lenaerts*[1]

[1] Sustainable Energy, Air and Water Technology (DuEL), Department of Bioscience Engineering, University of Antwerp, Groenenborgerlaan 171, B-2020 Antwerp, Belgium

* Sammy.verbruggen@uantwerp.be

[2] Center for Surface Chemistry and Catalysis, Department of Microbial and Molecular Systems, KU Leuven, Celestijnenlaan 200F, B-3001 Heverlee (Leuven), Belgium

Graphical abstract

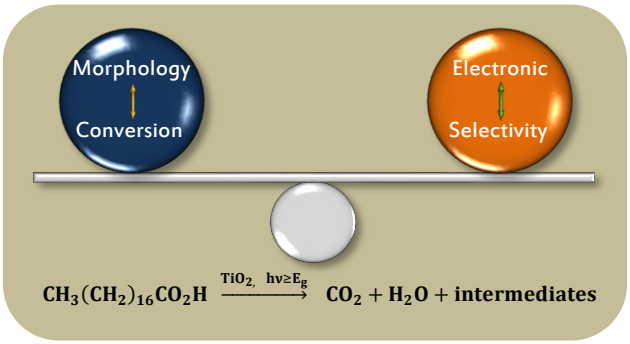

ABSTRACT

In this paper a structure-activity and -selectivity relation is established for three commercial TiO_2 sources (P25, P90, PC500). Morphological and electronic parameters of the photocatalysts are determined using widely applicable and inexpensive characterization procedures. More specifically, the electronic properties are rigorously characterized using an electron titration method yielding quantitative information on the amount of defect sites present in the catalyst. Surface photovoltage measurements on the other hand provide complementary information on the charge carrier recombination process. As model reaction, the degradation of a solid layer of stearic acid is studied using an in-situ FTIR reaction cell that enables to investigate the catalyst surface and possible formation of reaction intermediates while the reactions are ongoing. We show that the order of photocatalytic conversion is: PC500 > P90 > P25, matching the order of favorable morphological properties. In terms of selectivity to CO_2 formation (complete mineralization), however, this trend is reversed: P25 > P90 > PC500, now matching the order of advantageous electronic properties, i.e. low charge carrier recombination and high charge carrier generation. With this we intend to provide new mechanistic insights using a wide variety of physical, (wet) chemical and operando analysis methods that aid the development of performant (self-cleaning) photocatalytic materials.

KEYWORDS

Photocatalysis, titanium dioxide (TiO_2), structure-activity relation, stearic acid, in-situ FTIR, selectivity, electron titration, surface photovoltage, self-cleaning

1. INTRODUCTION

Photocatalysis is a well-established technology for pollution abatement in both the gas and aqueous phase.[1–4] More recently, photocatalytic self-cleaning materials have become an important application field as well.[5] In the selection of the most suitable catalyst, not only high activity but also pricing and safety play an important role. In this regard titanium dioxide (TiO_2) is an ideal candidate since it is relatively inexpensive, non-toxic, (photo-)stable and easily activated under UV light illumination.[6] In addition, it is already used in a number of everyday applications like the food industry, sunscreen, paint and cosmetics, that could facilitate rapid transition of self-cleaning TiO_2 applications from the laboratory scale to commercial applications.[5] One of the major drawbacks of TiO_2 based photocatalysis is its low efficiency, which is mainly due to charge carrier recombination. This problem can be circumvented by improving the photo-electronic properties or by modifying the photocatalyst on the morphological level.[7] The former involves the formation of composite semiconductors, doping or modification with (noble) metal nanoparticles.[8] The latter is mainly based on maximizing the exposure of the catalyst surface to pollutants by increasing the surface area using different (nanosized) geometries.[9] An additional advantage is that charge carriers are formed closer to the surface thus reducing charge carrier recombination.[7,10] It is evident that different factors play an important role and understanding the interplay between these phenomena is essential for further optimizing the photocatalytic efficiency. One should also keep in mind the final application. It is shown that the material properties that dominate the overall photocatalytic activity in aqueous phase differ from those in gas phase.[11–13] On the

55 other hand, very limited information is available on the driving properties for self-cleaning
56 applications taking place at the solid (catalyst) - solid (pollutant) - gas (ambient) interface.
57 In this study both morphological and electronic properties of three commercially available
58 photocatalysts are rigorously characterized in order to adequately evaluate the photocatalytic
59 self-cleaning activity and thus establish a full structure-activity relation. A valuable correlation
60 between photocatalytic activity and structural and physical properties of commercial TiO_2 has
61 been established by Ohtani's group using statistical multivariable analysis.[13] They used five
62 different representative reactions and their relative rates were linked to six different material
63 properties. Since all reactions were conducted in aqueous or gas phase, no conclusions can be
64 made on the driving factors of self-cleaning photocatalytic materials. The electronic properties
65 of photocatalysts can be studied using different (fundamental) spectroscopic techniques like
66 electron paramagnetic spectroscopy (EPR),[14–16] time resolved microwave conductivity
67 (TRMC) measurements,[17] photoacoustic spectroscopy (PAS)[18,19] and other ultrafast
68 spectroscopic techniques.[20–22] While these techniques yield insightful information, they
69 require dedicated expensive equipment and often tedious and complex sample preparation
70 steps. In this work it is our intent to use simple, widely applicable and inexpensive
71 characterization procedures that yield all the information required. More in particular, we used
72 a facile and fast characterization technique based on an adapted electron titration method
73 using a thiazine dye (thionine) yielding information on the electronic properties of powder TiO_2
74 samples. This electron titration method is based on the generation and storage (trapping) of
75 electrons of irradiated TiO_2 colloids in de-aerated conditions in the presence of a hole
76 scavenger. UV excitation of TiO_2 in de-aerated ethanol renders the suspension blue, which is

attributed to trapping of electrons at Ti^{4+} sites. This electron excess can be titrated using a suitable acceptor molecule like thionine. Because of the charging effect and the possibility to titrate the excess charge, it is possible to quantify the number of electrons stored on the TiO_2 particles.[23–30] The abovementioned electron titration method is thus used to evaluate the electronic properties of different commercially available TiO_2 photocatalysts. These results are complemented by direct surface photovoltage (SPV) measurements and morphological characterization data. Further linking the electronic and morphological characteristics of the samples to their ability to degrade a solid layer of stearic acid (SA), enables us to interpret the photocatalytic self-cleaning behavior of the investigated catalysts.

2. EXPERIMENTAL

2.1 Chemical reagents

All products were used as received from the manufacturers without any modification or purification unless stated otherwise. Three commercially available TiO_2 sources were used: Aeroxide P25 (Evonik), Aeroxide P90 (Evonik) and PC500 (CristalACTiV). All other chemicals were purchased from Emplura or Sigma-Aldrich.

2.2 Photocatalyst characterization

X-ray powder diffraction (XRD) measurements were conducted using a STOE StadiP apparatus with CuKα radiation and an image plate detector. The Brunauer-Emmett-Teller (BET) specific surface area was determined via N_2 adsorption with a Micromeritics Tristar Surface Area and Porosity Analyzer. The samples were first degassed overnight at 573 K. A filler rod and isothermal jacket were used during the measurements.

The amount of electrons stored on TiO_2 was determined quantitatively using thionine acetate salt (Sigma-Aldrich) as electron acceptor. 0.625 mg TiO_2 powder was suspended in 5 mL absolute ethanol (Emplura, 99.5%) in an airtight reaction vessel and de-aerated with N_2. The weight before and after the de-aeration step was measured to account for volume losses. The reaction vessel was subsequently illuminated with a low-intensity UVA lamp (λ_{max} = 352 nm, 5.3 ± 0.3 mW cm^{-2} at sample distance) for one hour while stirring. The holes are readily scavenged by the organic solvent and the suspension turns grayish-blue, which indicates the formation of electron-rich TiO_2. Afterwards, 1 mL of a de-aerated aqueous solution of thionine (0.1 mM) was added to the reduced TiO_2 suspension causing the stored electrons to reduce the thionine dye (blue) to its colorless *leuco*-thionine form. The resulting suspension was centrifuged for 20 minutes at 6000 rpm to eliminate the photocatalyst, after which the supernatant was loaded in a sealable quartz cell (optical path length 10 mm) and the UV-VIS absorption at 602.5 nm was measured using a Shimadzu UV-VIS 2501PC double beam spectrophotometer. To exclude the adverse effect of oxygen, all experiments were entirely conducted under N_2 atmosphere (two-hand Atmosbag with zipper lock, Sigma-Aldrich). Blanc samples were measured to correct for dye adsorption on the TiO_2 catalyst. These samples underwent the same experimental procedure but were shielded from UV light illumination using aluminum foil.

Surface photovoltage measurements were conducted as described by Verbruggen et al.[12] using a custom made apparatus where the catalyst powder is sandwiched between two ITO electrodes (Sigma-Aldrich, d = 1.2 mm, resistivity: 8-12 Ω cm^{-2}), connected to an amplifier (1 x 10^6 voltage amplification). No external bias was applied. For all samples, 4.0 ± 0.1 mg TiO_2

120 powder was used in such a way that a controlled area of 5 mm by 5 mm was illuminated with
121 UVA light (λ_{max} = 352 nm, 1.8 mW cm^{-2} at sample distance).
122
123 **2.3 Photocatalytic self-cleaning activity measurement**
124 The photocatalytic self-cleaning test was conducted by means of an in-situ stearic acid (SA)
125 degradation experiment, based on the method proposed by Paz et al.[31] Silicon wafers (1.5 cm
126 x 1.5 cm) were ultrasonically cleaned in ethanol and dried with compressed air. Afterwards, a 2
127 wt% TiO_2 suspension in absolute ethanol was prepared of which 25 µL was drop casted on the
128 silicon wafer. The coated wafers were subsequently dried overnight at 363 K. A layer of stearic
129 acid (Sigma-Aldrich, 98.5%) was applied by spin coating 50 µL of a 0.25 wt% stearic acid solution
130 in chloroform (Sigma-Aldrich, 99.8%) for 1 minute at 1000 rpm after which the samples were
131 dried for 15 minutes at 363 K. The photocatalytic degradation of stearic acid was monitored by
132 means of FTIR spectroscopy using a patented in-situ reaction cell developed in our research
133 group.[32] This cell enables the in-situ observation of volatile and non-volatile reagents,
134 intermediates and products on the surface while the reactions are ongoing. The samples were
135 placed in the center of the reactor at an angle of 9° with the IR beam to minimize internal
136 reflection effects. During the experiments, IR spectra were recorded from 4000 - 400 cm^{-1} at a
137 resolution of 1 cm^{-1} by a Thermo Nicolet 6700 spectrometer (Thermo Fisher Scientific). The
138 reactor was first flushed with air after which it was sealed airtight and the sample was allowed
139 to equilibrate for one hour. An average of eight spectra was logged every three minutes using
140 an automated protocol (MacrosBasic, Thermo Fisher) and the built-in UV LEDs (λ_{max} = 377 nm,
141 1.8 mW cm^{-2} at sample distance) were switched on. The disappearance of stearic acid was

followed by monitoring the integrated area in the wavenumber range 3000 - 2800 cm^{-1}, corresponding to the asymmetric $\nu_{as}(CH_3)$ in-plane C-H stretch at 2958 cm^{-1}, an asymmetric $\nu_{as}(CH_2)$ in-plane C-H stretch at 2923 cm^{-1} and a symmetric $\nu_s(CH_2)$ in-plane C-H stretch at 2853 cm^{-1}.[33] The concomitant formation of CO_2 and CO was monitored following the peak height of the asymmetric stretch $\nu_{as}(CO_2)$ at 2360 cm^{-1} and the stretch ν(CO) at 2179 cm^{-1} respectively.

3. RESULTS AND DISCUSSION

3.1 Morphological parameter characterization

An overview of the main important morphological material properties is given in Table 1. The surface area was determined by means of N_2 adsorption/desorption measurements by applying the BET method. XRD measurements were used to determine the crystallinity/crystal phases as well as the primary crystallite size.

Table 1. Overview of important morphological properties of the three commercial TiO_2 sources.

TiO_2 source	Surface area ($m^2 g^{-1}$)	Primary crystallite size[a] (nm)	Crystallinity
P25	59	18.8	85.6 wt% anatase 14.4 wt% rutile[b]
P90	125	10.9	89.3 wt% anatase 10.7 wt% rutile[b]
PC500	352	6.5	85 wt% anatase 15 wt% amorphous[c]

[a] Primary crystallite size of the dominant crystal phase (anatase), determined using the Scherrer equation.
[b] Determined with the formula of Spurr and Myers using the intensity of the strongest anatase and rutile peaks, being 25.28° and 27.4° 2θ.[34]
[c] As obtained from the manufacturer data.

3.2 Electronic parameter characterization

Determination of defect states using electron titration method

As indicated in the introduction, it is our intent to use simple and inexpensive characterization procedures without having to compromise on accuracy and precision. To probe the electronic properties of the catalysts we therefore propose a modified electron titration technique that enables quantitative analysis of defect sites, thereby gaining more information on the electron-hole pair (e^--h^+) recombination process. The method is based on the light-induced accumulation of electrons on TiO_2 powder in a de-aerated solution in the presence of a hole scavenger. In Figure 1 (a) equal amounts of TiO_2 powder are suspended in de-aerated ethanol. The left reaction vessel was illuminated by UV light, while the right vessel was shielded from illumination using aluminum foil. Charge separation takes place in the illuminated sample where the holes are scavenged by the organic solvent, causing the electrons to be trapped at Ti^{4+} forming Ti^{3+}, i.e. the electrons accumulate on the TiO_2 powder in the form of Ti^{3+}.[27] This can be verified macroscopically by the appearance of a distinct grayish-blue color (Figure 1 (a)). It is possible to determine the concentration of these accumulated electrons using thionine (TH) as acceptor molecule. Thionine exists as a monovalent cation and is readily reduced to its colorless *leuco* form (TH^{2-}) via a two-step reduction, as can be derived from reactions (1) and (2).[28,29]

$$2Ti^{3+} + 2TH_{(blue)} \rightarrow 2Ti^{4+} + 2TH^{-} \qquad (1)$$

$$2TH^{-} \rightarrow TH^{2-}_{(colorless)} + TH \qquad (2)$$

In order for this reaction to occur spontaneously, the reductive power of the trapped electrons should be strong enough, i.e. the defective sites should have a more negative electrochemical potential than the TH/TH^{2-} redox couple. The redox potential of the dye used in this study is +0.064 V vs. NHE.[29] Assuming the accumulated electrons are trapped just below the conduction band edge of TiO_2 (-0.52 V vs. NHE[35]), the stored electrons will indeed react readily with the thionine molecules, reducing them to their colorless form (reactions (1) and (2)). This can be seen in Figure 1 (b). A known amount of a de-aerated thionine dye solution is added to both reaction vessels. In the previously irradiated TiO_2 suspension (left), the stored electrons reduce the dye to its colorless form, causing the grayish-blue color (indicative of electron storage) to disappear. The non-illuminated reaction vessel (right) attains the dark blue color of the thionine dye solution. Using the extinction band of thionine at 602.5 nm ($\varepsilon_{thionine}$ in a five-to-one ethanol/water mixture is determined to be 81800 M^{-1} cm^{-1}), it is possible to determine the amount of thionine molecules that are reduced. The reader is referred to Figure S1 in the supplementary information for the UV-VIS absorption spectra of the thionine dye before and after reduction to its colorless form.

Keeping in mind that two electrons are needed to bleach one thionine molecule, the amount of trapped electrons can thus be calculated. It is important to note that both the stored electrons on TiO_2 and the reduced *leuco* form of the dye are highly stable under inert atmosphere but are easily oxidized by coexisting oxygen in the solution (Figure 1 (c) and (d)). Even small amounts of O_2 present during the measurement would result in quenching of the signal and consequently lead to large experimental errors. The errors on the values we obtained are quite low (Figure 2), demonstrating the high accuracy and reproducibility of the

electron titration method. Our values are also in the same order of magnitude as the ones found in literature by applying a comparable analysis.[13,23,27] For instance, Prieto-Mahaney et al.[13] determined the molar amount of defective sites for commercially available P25 to be 59 µmol g^{-1}, which is somewhat lower than the value of 95 µmol g^{-1} that we obtained. They used triethanolamine as hole scavenger and methyl viologen as titrant. The redox potential of methyl viologen is -0.45 V vs. NHE (as compared to +0.064 V vs. NHE for thionine) so it is likely that the reductive power of some deeper trapped electrons is not sufficient to reduce the methyl viologen, resulting in a slightly lower value than the one obtained in our study. In general, such a high number of defects can be largely attributed to the co-existence of different crystalline phases in the sample and its nanostructured nature.

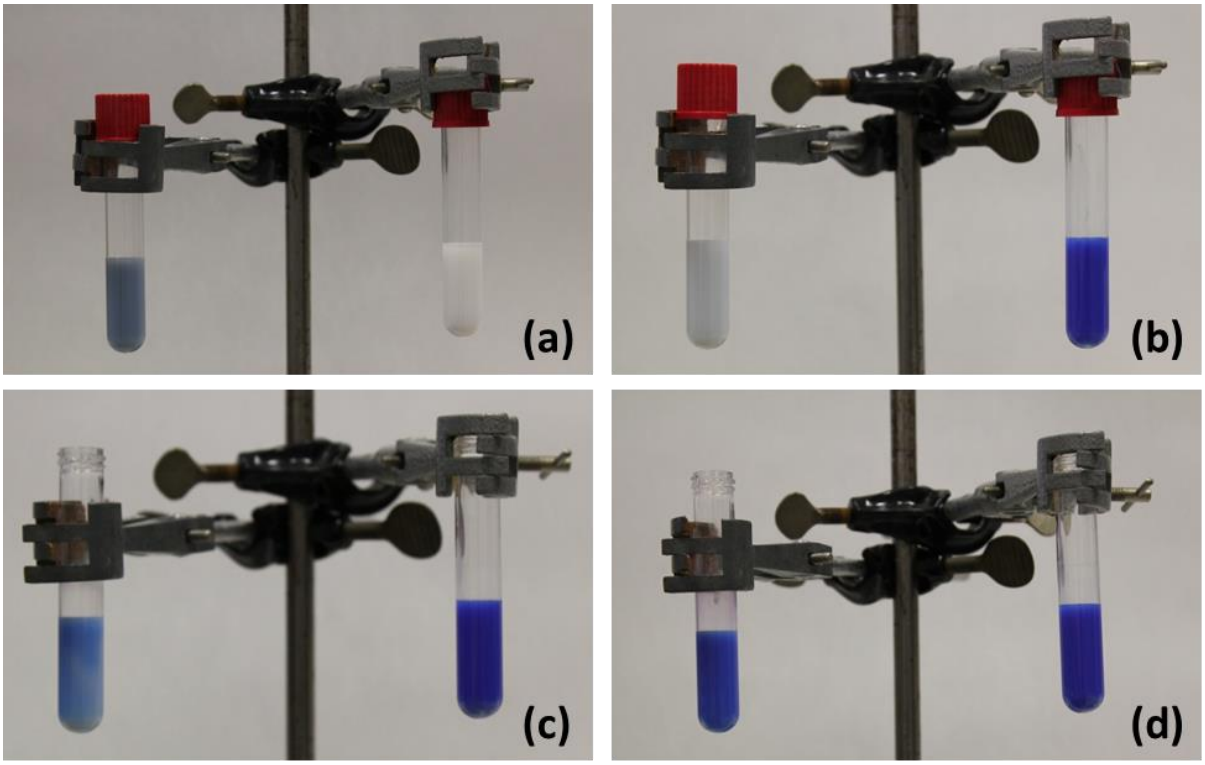

Figure 1. Overview of the different steps taking place during the photocatalytic electron titration experiment. (a) Equal amounts of TiO_2 were suspended in de-aerated ethanol. The left reaction vessel was illuminated with UV

light causing the electrons to accumulate on the powder and the suspension to turn grayish-blue. (b) Situation after addition of equal amounts of a de-aerated aqueous thionine solution. The stored electrons in the left reaction vessel reduce the dye to its colorless form. In the right reaction vessel no dye reduction takes place, thus the suspension gets the dark blue color of the stock thionine solution. (c) Effect of the presence of oxygen five minutes after opening the reaction vessel. The colorless *leuco*-thionine (left reaction vessel) reverts to its original colored form. (d) Effect of the presence of oxygen 20 minutes after opening the reaction vessel.

From our analysis it can be derived that the capacity for electron trapping follows the order PC500 > P90 > P25 (Figure 2). A study by Ikeda et al.[27] suggests that the formed Ti^{3+} species are produced by trapping electrons at – and thus quantify the number of – defect sites in TiO_2. Since electron-hole pair recombination is facilitated by defects,[8] it can be stated that the electron titration method directly yields information on the recombination process and therefore also on the charge carrier formation efficiency. They demonstrated a linear correlation between the rate of e^--h^+ pair recombination and the molar amount of defective sites per unit weight of TiO_2 powder. Considering our results, this implies that P25 is less prone to charge carrier recombination than P90 and PC500 and thus is the most favorable photocatalyst in terms of electronic properties.

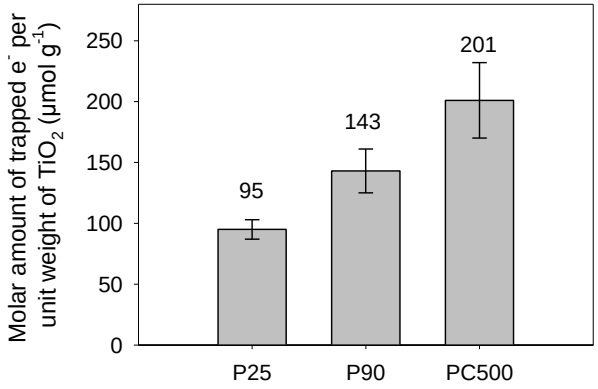

Figure 2. Molar amount of trapped electrons per unit weight for the three commercial TiO_2 powders.

Surface photovoltage (SPV) measurements

Surface photovoltage (SPV) measurements enable a detailed characterization of semiconductors yielding complementary information on the electronic properties. The technique is based on an illumination-induced change in the surface photovoltage.[36] Contact between a semiconductor and a conductor leads to the formation of a non-neutral space charge region near the surface that in turn gives rise to a built-in electric field, commonly referred to as the surface potential barrier. When the semiconductor is illuminated by UV light, free charge carriers are generated which will redistribute because of the built-in electric field. This will alter the surface potential barrier. The difference in surface potential before and during illumination is defined as the SPV signal.[12,37] The amount of charge carriers formed is directly related to the potential difference and thus the SPV signal. Therefore, SPV measurements provide valuable information on the charge carrier formation efficiency of the semiconductor. The technique has many similarities to the aforementioned electron titration procedure as it is also fast, simple, cheap, directly applicable to powders and does not require any sample preparation. Therefore, SPV is an ideal candidate to corroborate and further complement the results of our adapted electron titration method. The SPV signal of the three commercial TiO_2 sources can be found in Figure 3.

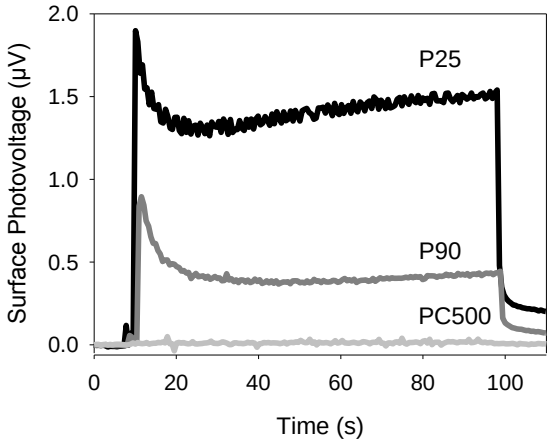

Figure 3. Surface photovoltage measurements for P25 (black), P90 (dark gray) and PC500 (light gray). Light was switched on after 10 s and turned off at 100 s (sample was illuminated for 90 s).

P25 displays the highest SPV signal and thus the best charge carrier formation efficiency whereas the signal of PC500 is negligible. These results are in excellent agreement with the results obtained by the electron titration method (*vide supra*) according to which P25 has the least amount of defect states and is therefore less susceptible to charge carrier recombination. PC500 on the other hand only generates a poor amount of stable charge carriers, as it is more prone to charge carrier recombination (evidenced by the electron titration experiment), probably due to the large amount of non-crystalline material present in the sample (Table 1).

3.3 In-situ investigation of the photocatalytic self-cleaning activity

The degradation of a solid layer of stearic acid (SA) is a commonly accepted method to assess the self-cleaning photocatalytic activity.[31,38–41] SA is a photo-stable model compound for organic fouling on both interior and exterior surfaces. In this method, a thin layer of SA is deposited onto the photocatalyst and its destruction over time is monitored by means of FTIR since the molecule absorbs strongly in the region from 3000 to 2800 cm^{-1}. Complete

mineralization of SA to CO_2 can be achieved as was evidenced by Mills and Wang who followed the simultaneous decrease of SA and increase in CO_2.[33] In the present research, the photocatalytic degradation of SA was monitored using a reaction cell developed in our research group that enables the in-situ monitoring of the catalyst surface, while the reaction is ongoing. The decrease of the FTIR absorption band of SA from 3000 - 2800 cm^{-1} during UV illumination corresponding to the decrease of number of SA molecules is shown for the three commercial TiO_2 sources as a function of illumination time in Figure 4 (a) and (b).

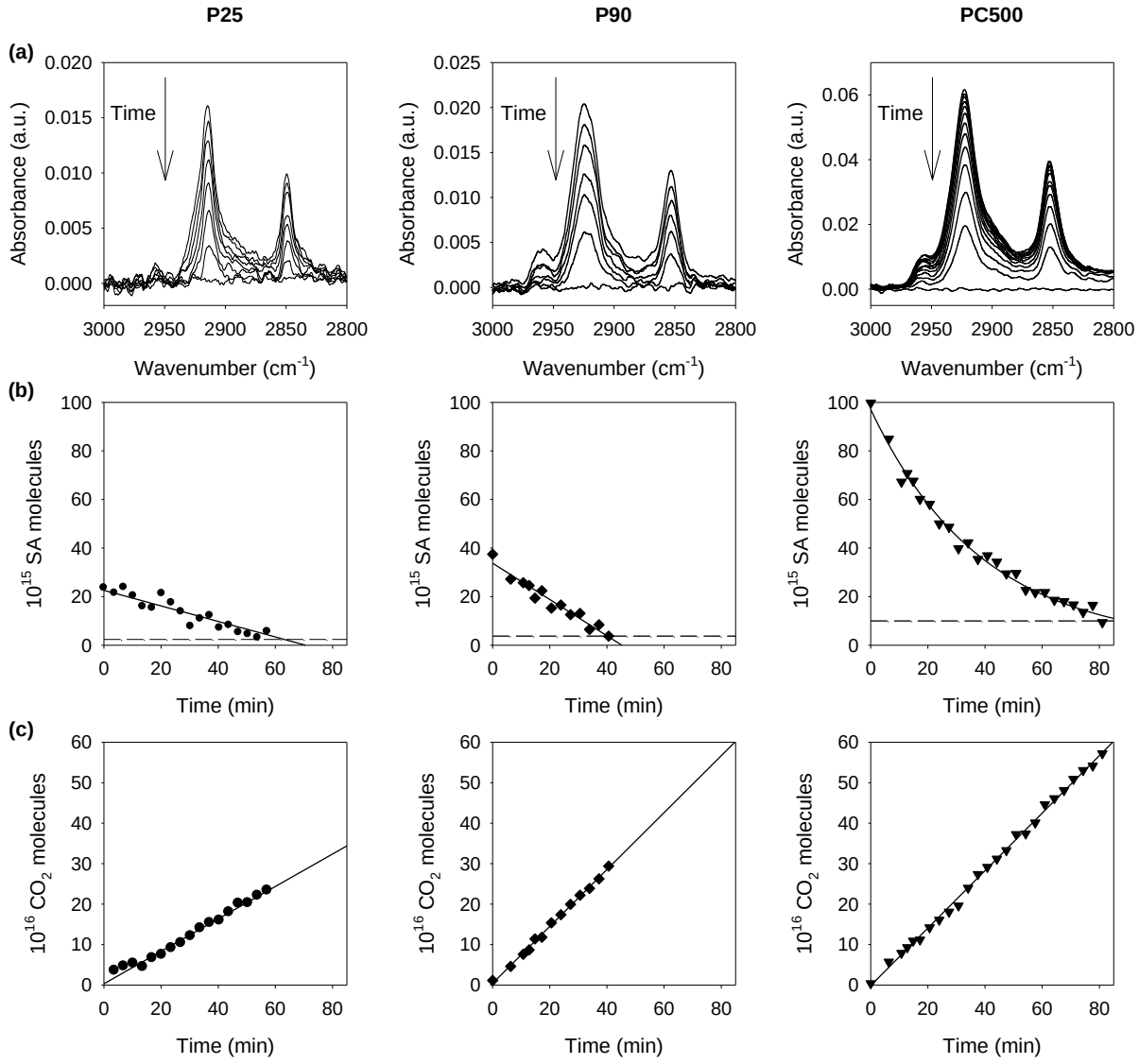

Figure 4. (a) Decrease of FTIR absorption bands of SA in the range of 3000 - 2800 cm^{-1} during UV illumination. (b) Decrease of SA molecules over time, determined from the integrated area from 3000 - 2800 cm^{-1} under the corresponding curves of Figure 1 (a). The values are shown until only 10% of the original SA concentration was present (dashed curve). The kinetic models (solid lines) are also based on the first 90% of conversion. (c) CO_2 formation in function of illumination time during the first 90% of SA conversion.

Since SA appears as a transparent coating over the photocatalyst, light absorption by the pollutant can be neglected in the kinetic pathway. Depending on the porosity of the photocatalyst layer, zero or first order kinetics can be expected. It is shown by Ollis that for non-porous catalyst layers a zero order kinetic model satisfactorily describes the SA degradation rate, while in the case of a porous catalyst layer, apparent first order behavior can be expected.[42] Both situations apply in our results, as can be seen in Figure 4 (b). P25 and P90 films exhibit zero order kinetics while PC500 clearly shows first order behavior. Still, both sample preparation and activity measurement were identical for all three TiO_2 sources. The PC500 film, however, appeared to be much coarser, consisting of aggregated islands, whereas P25 and P90 layers were much more uniform. This intrinsic difference in overall layer morphology can explain the different kinetic behavior of the PC500 sample that acts as a porous film, leading to first order kinetics. Despite the difference in kinetic order, in terms of the disappearance rate of SA, it is clear that the PC500 film is most active while P25 exhibits the lowest photocatalytic self-cleaning activity.

To enable a more appropriate, quantitative, comparison of the full mineralization activity, the CO_2 formation was also studied by monitoring the peak height of the asymmetric stretch $\nu_{as}(CO_2)$ at 2360 cm^{-1} over time. These results are shown in Figure 4 (c). It can be seen that the CO_2 formation rate increases linearly with illumination time for all three samples. P25 is the

294 least active catalyst, which is in agreement with the SA removal results. Remarkably, there is no
295 longer any difference in activity between P90 and PC500. The PC500 sample also shows a clear
296 linear relationship between CO_2 formation and illumination time, as opposed to its first order
297 SA removal kinetics. This indicates that for these PC500 films the initial oxidation process
298 proceeds fast but gives rise to long lived intermediates which are harder to degrade. Minabe et
299 al. studied the photocatalytic decomposition of SA by TiO_2 and found that they could only
300 remove 69% of the original amount of SA, also pointing to the formation of intermediates that
301 are less easily degraded.[43] Since the in-situ reaction cell used in our experiments enables to
302 monitor the surface while the reactions are ongoing, the FTIR spectra were carefully examined
303 to see whether some intermediates could be observed. Figure 5 shows the FTIR spectrum of
304 PC500 in the range of 1900 to 1200 cm^{-1} after 90% of the SA was converted. The negative
305 absorbance from 1530 to 1430 cm^{-1} is attributed to the disappearance of stearic acid from the
306 surface. It is evident from this spectrum that different intermediates like acetaldehyde,
307 formaldehyde and their oxidation products (acetate, formate) are indeed present on the
308 surface. Assignment of the different bands can be found in Table 2. These results are in good
309 agreement with those obtained by Roméas et al.[44] who studied the photomineralization of
310 palmitic acid by TiO_2 coated self-cleaning glass. They found there was a negative deviation of
311 the expected reaction stoichiometry due to the formation of intermediates like acetone,
312 acetaldehyde and formaldehyde.

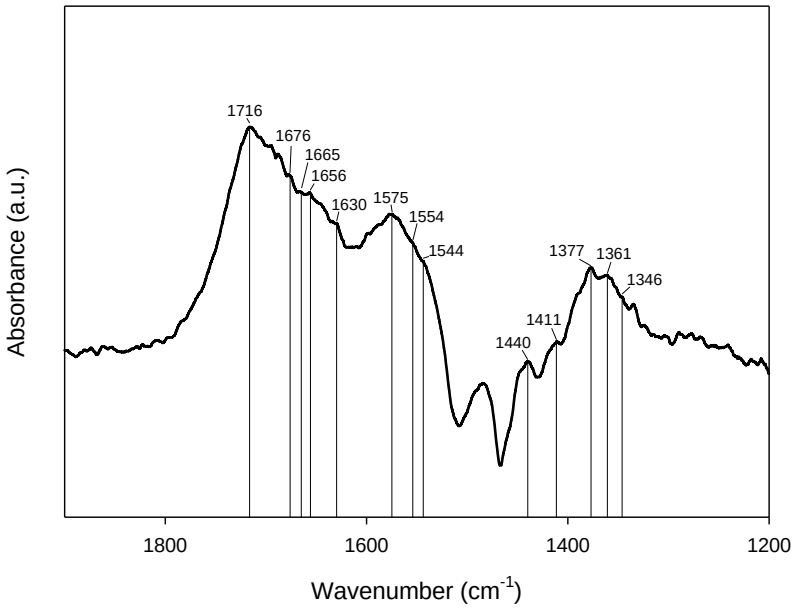

313

314 **Figure 5.** IR spectrum of PC500 (after H_2O correction) after 90% of SA was removed by UV light illumination.

315 **Table 2.** Assignment of the FTIR bands observed on the surface of PC500 after 90% of SA was removed.

Adsorbed molecule	Vibration mode	Frequency (cm^{-1})	
		Literature[45]	This work
$HCOOH_{ad}$	ν(C=O)	1713	1716
CH_3COOH_{ad}	ν(C=O)	1675	1676
$HCHO_{ad}$	ν(C=O)	1662	1665
CH_3CHO_{ad}	ν(C=O)	1653	1656
CH_3CHO_{ad}	ν(C=C)	1625	1630
$HCOO^-_{ad}$	ν_{as}(COO)	1574	1575
$HCOO^-_{ad}$	ν_{as}(COO)	1554	1554
$CH_3COO^-_{ad}$	ν_{as}(COO)	1547	1544
CH_3CHO_{ad}	$\delta_{as}(CH_3)$	1444	1440
$HCOO^-_{ad}$	δ(CH)	1416	1411

$HCOO^-_{ad}$	$\nu_s(COO)$	1378	1377
$HCOO^-_{ad}$	$\nu_s(COO)$	1357	1361
$CH_3COO^-_{ad}$	$\delta_{as}(CH_{3)}$	1343	1346

316

317 Complete mineralization of one SA molecule yields 18 molecules of CO_2. Since some long-
318 lived intermediates are formed in our experiments, the SA:CO_2 ratio will be lower than the
319 reaction stoichiometry value of 1:18 i.e. the selectivity toward CO_2 formation will deviate from
320 unity. This drop in selectivity has also been determined in our experiments and is plotted in
321 Figure 6. Even though PC500 is the most active catalyst to remove a solid layer of SA, it has the
322 lowest selectivity toward CO_2 formation (37%). P25, the least active catalyst, on the other hand
323 has a selectivity of 60%, meaning that 11 CO_2 molecules are formed per SA molecule. Mills and
324 Wang also tested the SA degradation capacity of P25 and observed the same drop in the SA:CO_2
325 stoichiometric ratio from 1:18 to 1:12 (corresponding to a selectivity of 69%) after ca. 50
326 minutes of irradiation.[33] This value matches quite well with the selectivity obtained for P25 in
327 our study.

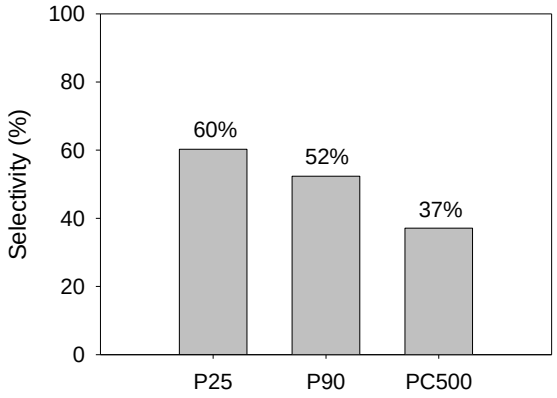

328

Figure 6. Selectivity toward CO_2 formation for the three tested samples. A selectivity of 100% means full mineralization of SA to CO_2 is achieved resulting in a SA:CO_2 ratio of 1:18.

3.4 Discussion on the structure-activity-selectivity relation

Based on the characterization of the electronic photocatalyst properties (electron titration + SPV), it is expected that P25 shows the highest photocatalytic activity since its (photo)electronic properties outperform those of P90 and PC500.[11,12] It has the lowest amount of defect/recombination sites and the highest SPV value, indicating a good charge carrier formation efficiency and subsequently high photocatalytic activity. This can be explained by the fact that P25 is characterized by a high quantum efficiency because of its fully crystalline nature (few surface and bulk defects[11]), as opposed to PC500 (15 wt% amorphous). In addition, the superior activity of commercial P25 is often attributed to its polymorphic composition (85 wt% anatase, 15 wt% rutile) that ameliorates charge separation due to the favorable position of the valence and conduction bands of both crystal phases. P90 is also fully crystalline but has a different anatase to rutile ratio (90 wt% anatase, 10 wt% rutile) that deviates more from the optimal composition found by Su et al. (60 wt% anatase and 40 wt% rutile).[46] In terms of morphological properties on the other hand, PC500 stands out since it has the smallest primary particle size and the highest surface area (6 times higher than P25, 3 times higher than P90).

Linking both morphological and electronic material properties to the ability to convert a solid layer of stearic acid for the three commercial TiO_2 sources, it can be concluded that not the electronic properties but mainly the high surface area is the driving factor for self-cleaning applications. P25 clearly outperforms P90 and PC500 in terms of charge carrier formation efficiency but has the lowest activity. PC500 on the other hand displays the largest surface area

and also has the highest photocatalytic activity. These results agree well with an earlier study by our group where PC500 outperforms P90 and P25 for the degradation of acetaldehyde in air.[12] Interestingly, the trend is reversed for photocatalytic activity measurements in aqueous phase, were P25 excels over P90 and PC500. During gas phase measurements, the (small) gaseous pollutants can access the entire surface whereas pollutants in aqueous phase are hindered by diffusion limitations. A large surface area consisting of small pores is thus only desirable when mass transfer limitations can be neglected.[12] The consistency between the driving factors of gas phase photocatalysis and self-cleaning applications can be rationalized well: The photocatalytic oxidation of organic solids can be considered as a special border case of gas phase photocatalysis, as the reactions take place at the solid (catalyst) - solid (pollutant) - gas (ambient) interface. In addition, the supply of O_2 and the removal of CO_2 follow the same mass transfer laws as those of gas phase reactions, without being obstructed by a liquid barrier giving rise to diffusion limitations.[7]

Next to activity, selectivity is also an important catalyst property. When looking at the ability to fully mineralize the pollutant, i.e. obtaining high selectivity toward CO_2, the trend in photocatalytic activity (PC500 > P90 > P25) is reversed! It can indeed be concluded from Figure 6 that P25 has the highest mineralization efficiency (60%), followed by P90 (52%) and PC500 (37%). Interestingly, this reversed trend corresponds well with the trend observed in the electronic parameter characterization (P25 > P90 > PC500). It can thus be concluded that in terms of photocatalytic self-cleaning *activity*, the morphological properties present the driving parameters. If we however take a look at mineralization *selectivity*, the electronic properties play a more prominent role. PC500 (largest surface area, least favorable electronic properties)

thus has the highest self-cleaning activity i.e. can initially convert the most SA molecules because of the high amount of active sites. The initial conversion however gives rise to some long-lived intermediates on the surface that prove to be more difficult to degrade. P25 on the other hand (lowest specific surface area, best electronic properties) has less active sites so can convert less SA molecules, but because of its desirable electronic properties is able to mineralize the pollutant more selectively to CO_2.

4. CONCLUSION

In order to properly assess the photocatalytic properties of self-cleaning TiO_2, rigorous multi-aspect characterization is key since differences in macroscopic activity measurements cannot always be attributed to a single material property. For this reason, we conducted a full morphological and electronic characterization of three commercial TiO_2 photocatalysts (P25, P90, PC500) to obtain a coherent structure-activity and -selectivity relation for self-cleaning applications. Our results indicate that P25 has the most desirable electronic properties compared to P90 and PC500 but is outperformed by PC500 and P90 in terms of morphological properties. These favorable morphological properties were shown to lead to a high photocatalytic self-cleaning activity. The opposite is true when looking at selectivity, where good electronic properties are the predominant factor. The obtained structure-activity-selectivity relation provides more mechanistic insight in the self-cleaning behavior of photocatalytic surfaces. We are hopeful this will boost the development of high-performant photocatalytic self-cleaning materials and facilitate a rapid transition from the laboratory scale to commercial applications.

ACKNOWLEDGEMENTS

M.K. acknowledges Flemish Agency for Innovation & Entrepreneurship for the doctoral scholarship. S.W.V. acknowledges the Research Foundation-Flanders (FWO) for a postdoctoral fellowship. J.A.M. acknowledges the Flemish government for long-term structural funding (Methusalem).

REFERENCES

[1] J.-M. Herrmann, Heterogeneous photocatalysis: fundamentals and applications to the removal of various types of aqueous pollutants, Catal. Today. 53 (1999) 115–129. doi:10.1016/S0920-5861(99)00107-8.

[2] U.I. Gaya, A.H. Abdullah, Heterogeneous photocatalytic degradation of organic contaminants over titanium dioxide: A review of fundamentals, progress and problems, J. Photochem. Photobiol. C Photochem. Rev. 9 (2008) 1–12. doi:10.1016/j.jphotochemrev.2007.12.003.

[3] S.W. Verbruggen, S. Ribbens, T. Tytgat, B. Hauchecorne, M. Smits, V. Meynen, P. Cool, J.A. Martens, S. Lenaerts, The benefit of glass bead supports for efficient gas phase photocatalysis: Case study of a commercial and a synthesised photocatalyst, Chem. Eng. J. 174 (2011) 318–325. doi:10.1016/j.cej.2011.09.038.

[4] J. Peral, X. Domènech, D.F. Ollis, Heterogeneous photocatalysis for purification, decontamination and deodorization of air, J. Chem. Technol. Biotechnol. 70 (1997) 117–140. doi:10.1002/(SICI)1097-4660(199710)70:2<117::AID-JCTB746>3.0.CO;2-F.

[5] I.P. Parkin, R.G. Palgrave, Self-cleaning coatings, J. Mater. Chem. 15 (2005) 1689–1695. doi:10.1039/b412803f.

[6] O. Carp, C.L. Huisman, A. Reller, Photoinduced reactivity of titanium dioxide, Prog. Solid State Chem. 32 (2004) 33–177. doi:10.1016/j.progsolidstchem.2004.08.001.

[7] S.W. Verbruggen, TiO2 photocatalysis for the degradation of pollutants in gas phase: From morphological design to plasmonic enhancement, J. Photochem. Photobiol. C Photochem. Rev. 24 (2015) 64–82. doi:10.1016/j.jphotochemrev.2015.07.001.

[8] M. Pelaez, N.T. Nolan, S.C. Pillai, M.K. Seery, P. Falaras, A.G. Kontos, P.S.M. Dunlop, J.W.J. Hamilton, J.A. Byrne, K. O'Shea, M.H. Entezari, D.D. Dionysiou, A review on the visible light active titanium dioxide photocatalysts for environmental applications, Appl. Catal. B Environ. 125 (2012) 331–349. doi:10.1016/j.apcatb.2012.05.036.

[9] K. Nakata, A. Fujishima, TiO2 photocatalysis: Design and applications, J. Photochem. Photobiol. C Photochem. Rev. 13 (2012) 169–189. doi:10.1016/j.jphotochemrev.2012.06.001.

[10] R.M. Navarro Yerga, M.C. Álvarez Galván, F. del Valle, J.A. Villoria de la Mano, J.L.G. Fierro, Water Splitting on Semiconductor Catalysts under Visible-Light Irradiation, ChemSusChem. 2 (2009) 471–485. doi:10.1002/cssc.200900018.

[11] S.W. Verbruggen, K. Masschaele, E. Moortgat, T.E. Korany, B. Hauchecorne, J.A. Martens, S. Lenaerts, Factors driving the activity of commercial titanium dioxide powders towards gas phase photocatalytic oxidation of acetaldehyde, Catal. Sci. Technol. 2 (2012) 2311–2318. doi:10.1039/c2cy20123b.

[12] S.W. Verbruggen, J.J.J. Dirckx, J.A. Martens, S. Lenaerts, Surface photovoltage measurements: A quick assessment of the photocatalytic activity?, Catal. Today. 209 (2013) 215–220. doi:10.1016/j.cattod.2012.11.010.

[13] O.-O. Prieto-Mahaney, N. Murakami, R. Abe, B. Ohtani, Correlation between Photocatalytic Activities and Structural and Physical Properties of Titanium(IV) Oxide Powders, Chem. Lett. 38 (2009) 238–239. doi:10.1246/cl.2009.238.

[14] R.F. Howe, M. Grätzel, EPR observation of trapped electrons in colloidal TiO2, J. Phys. Chem. 89 (1985) 4495–4499. doi:10.1021/j100267a018.
[15] J.M. Coronado, A.J. Maira, J.C. Conesa, K.L. Yeung, V. Augugliaro, J. Soria, EPR study of the surface characteristics of nanostructured TiO2 under UV irradiation, Langmuir. 17 (2001) 5368–5374. doi:10.1021/la010153f.
[16] I. Caretti, M. Keulemans, S.W. Verbruggen, S. Lenaerts, S. Van Doorslaer, Light-Induced Processes in Plasmonic Gold/TiO2 Photocatalysts Studied by Electron Paramagnetic Resonance, Top. Catal. 58 (2015) 776–782. doi:10.1007/s11244-015-0419-4.
[17] C. Colbeau-Justin, M. Kunst, D. Huguenin, Structural influence on charge-carrier lifetimes in TiO2 powders studied by microwave absorption, J. Mater. Sci. 38 (2003) 2429–2437.
[18] N. Murakami, O.-O. Prieto-Mahaney, T. Torimoto, B. Ohtani, Photoacoustic spectroscopic analysis of photoinduced change in absorption of titanium(IV) oxide photocatalyst powders: A novel feasible technique for measurement of defect density, Chem. Phys. Lett. 426 (2006) 204–208. doi:10.1016/j.cplett.2006.06.001.
[19] N. Murakami, O.O. Prieto Mahaney, R. Abe, T. Torimoto, B. Ohtani, Double-Beam Photoacoustic Spectroscopic Studies on Transient Absorption of Titanium(IV) Oxide Photocatalyst Powders, J. Phys. Chem. C. 111 (2007) 11927–11935. doi:10.1021/jp071362x.
[20] B. Ohtani, R.M. Bowman, D.P. Colombo Jr., H. Kominami, H. Noguchi, K. Uosaki, Femtosecond Diffuse Reflectance Spectroscopy of Aqueous Titaniu(IV) Oxide Suspension: Correlation of Electron-Hole Recombination Kinetics with Photocatalytic Activity, Chem. Lett. 27 (1998) 579–580. doi:10.1246/cl.1998.579.
[21] S. Ikeda, N. Sugiyama, B. Pal, G. Marcí, L. Palmisano, H. Noguchi, K. Uosaki, B. Ohtani, Photocatalytic activity of transition-metal-loaded titanium(IV) oxide powders suspended in aqueous solutions: Correlation with electron–hole recombination kinetics, Phys. Chem. Chem. Phys. 3 (2001) 267–273. doi:10.1039/b008028o.
[22] T. Yoshihara, R. Katoh, A. Furube, Y. Tamaki, M. Murai, K. Hara, S. Murata, H. Arakawa, M. Tachiya, Identification of Reactive Species in Photoexcited Nanocrystalline TiO2 Films by Wide-Wavelength-Range (400-2500 nm) Transient Absorption Spectroscopy, J. Phys. Chem. B. 108 (2004) 3817–3823. doi:10.1021/jp031305d.
[23] B. Ohtani, Y. Ogawa, S. Nishimoto, Photocatalytic Activity of Amorphous-Anatase Mixture of Titanium(IV) Oxide Particles Suspended in Aqueous Solutions, J. Phys. Chem. B. 101 (1997) 3746–3752. doi:10.1021/jp962702+.
[24] A. Wood, M. Giersig, P. Mulvaney, Fermi level equilibration in quantum dot-metal nanojunctions, J. Phys. Chem. B. 105 (2001) 8810–8815. doi:10.1021/jp011576t.
[25] V. Subramanian, E.E. Wolf, P. V. Kamat, Green Emission to Probe Photoinduced Charging Events in ZnO−Au Nanoparticles. Charge Distribution and Fermi-Level Equilibration†, J. Phys. Chem. B. 107 (2003) 7479–7485. doi:10.1021/jp0275037.
[26] M. Jakob, H. Levanon, P. V. Kamat, Charge distribution between UV-irradiated TiO2 and gold nanoparticles: Determination of shift in the Fermi level, Nano Lett. 3 (2003) 353–358. doi:10.1021/nl0340071.
[27] S. Ikeda, N. Sugiyama, S. Murakami, H. Kominami, Y. Kera, H. Noguchi, K. Uosaki, T. Torimoto, B. Ohtani, Quantitative analysis of defective sites in titanium(IV) oxide photocatalyst powders, Phys. Chem. Chem. Phys. 5 (2003) 778–783.

doi:10.1039/b206594k.
[28] V. Subramanian, E.E. Wolf, P. V. Kamat, Catalysis with TiO2/Gold Nanocomposites. Effect of Metal Particle Size on the Fermi Level Equilibration, J. Am. Chem. Soc. 126 (2004) 4943–4950. doi:10.1021/ja0315199.
[29] A. Kongkanand, P. V. Kamat, Electron Storage in Single Wall Carbon Nanotubes. Fermi Level Equilibration in Semiconductor–SWCNT Suspensions, ACS Nano. 1 (2007) 13–21. doi:10.1021/nn700036f.
[30] A. Takai, P. V. Kamat, Capture, Store and Discharge. Shuttling Photogenerated Electrons across TiO2-Silver Interface, ACS Nano. 5 (2011) 7369–7376. doi:10.1021/nn202294b.
[31] Y. Paz, Z. Luo, L. Rabenberg, A. Heller, Photooxidative self-cleaning transparent titanium dioxide films on glass, J. Mater. Res. 10 (1995) 2842–2848. doi:10.1557/JMR.1995.2842.
[32] B. Hauchecorne, T. Tytgat, D. Terrens, F. Vanpachtenbeke, S. Lenaerts, Validation of a newly developed FTIR in situ reactor: Real time study of photocatalytic degradation of nitric oxide, Infrared Phys. Technol. 53 (2010) 469–473. doi:10.1016/j.infrared.2010.09.008.
[33] A. Mills, J. Wang, Simultaneous monitoring of the destruction of stearic acid and generation of carbon dioxide by self-cleaning semiconductor photocatalytic films, J. Photochem. Photobiol. A Chem. 182 (2006) 181–186. doi:10.1016/j.jphotochem.2006.02.010.
[34] R.A. Spurr, H. Myers, Quantitative Analysis of Anatase-Rutile Mixtures with an X-Ray Diffractometer, Anal. Chem. 29 (1957) 760–762. doi:10.1021/ac60125a006.
[35] A. Fujishima, T.N. Rao, D.A. Tryk, Titanium dioxide photocatalysis, J. Photochem. Photobiol. C Photochem. Rev. 1 (2000) 1–21.
[36] B. Xin, Z. Ren, P. Wang, J. Liu, L. Jing, H. Fu, Study on the mechanisms of photoinduced carriers separation and recombination for Fe3+-TiO2 photocatalysts, Appl. Surf. Sci. 253 (2007) 4390–4395. doi:10.1016/j.apsusc.2006.09.049.
[37] L. Kronik, Y. Shapira, Surface photovoltage spectroscopy of semiconductor structures: At the crossroads of physics, chemistry and electrical engineering, Surf. Interface Anal. 31 (2001) 954–965. doi:10.1002/sia.1132.
[38] E. Allain, S. Besson, C. Durand, M. Moreau, T. Gacoin, J.-P. Boilot, Transparent mesoporous nanocomposite films for self-cleaning applications, Adv. Funct. Mater. 17 (2007) 549–554. doi:10.1002/adfm.200600197.
[39] S.W. Verbruggen, M. Keulemans, B. Goris, N. Blommaerts, S. Bals, J.A. Martens, S. Lenaerts, Plasmonic “rainbow” photocatalyst with broadband solar light response for environmental applications, Appl. Catal. B Environ. 188 (2016) 147–153. doi:10.1016/j.apcatb.2016.02.002.
[40] S. Deng, S.W. Verbruggen, S. Lenaerts, J.A. Martens, S. Van Den Berghe, K. Devloo-Casier, W. Devulder, J. Dendooven, D. Deduytsche, C. Detavernier, Controllable nitrogen doping in as deposited TiO2 film and its effect on post deposition annealing, J. Vac. Sci. Technol. A. 32 (2014) 01A123. doi:10.1116/1.4847976.
[41] S.W. Verbruggen, M. Keulemans, M. Filippousi, D. Flahaut, G. Van Tendeloo, S. Lacombe, J.A. Martens, S. Lenaerts, Plasmonic gold–silver alloy on TiO2 photocatalysts with tunable visible light activity, Appl. Catal. B Environ. 156-157 (2014) 116–121. doi:10.1016/j.apcatb.2014.03.027.

[42] D. Ollis, Kinetics of photocatalyzed film removal on self-cleaning surfaces: Simple configurations and useful models, Appl. Catal. B Environ. 99 (2010) 478–484. doi:10.1016/j.apcatb.2010.06.029.
[43] T. Minabe, D.A. Tryk, P. Sawunyama, Y. Kikuchi, K. Hashimoto, A. Fujishima, TiO2-mediated photodegradation of liquid and solid organic compounds, J. Photochem. Photobiol. A Chem. 137 (2000) 53–62.
[44] V. Roméas, P. Pichat, C. Guillard, T. Chopin, C. Lehaut, Degradation of palmitic (hexadecanoic) acid deposited on self-cleaning glass: kinetics of disappearance, TiO2-coated intermediate products and degradation pathways, New J. Chem. 23 (1999) 365–373.
[45] B. Hauchecorne, D. Terrens, S. Verbruggen, J.A. Martens, H. Van Langenhove, K. Demeestere, S. Lenaerts, Elucidating the photocatalytic degradation pathway of acetaldehyde: An FTIR in situ study under atmospheric conditions, Appl. Catal. B Environ. 106 (2011) 630–638. doi:10.1016/j.apcatb.2011.06.026.
[46] R. Su, R. Bechstein, L. Sø, R.T. Vang, M. Sillassen, B. Esbjörnsson, A. Palmqvist, F. Besenbacher, How the Anatase-to-Rutile Ratio Influences the Photoreactivity of TiO2, J. Phys. Chem. C. 115 (2011) 24287–24292. doi:10.1021/jp2086768.